Using End-Confined Chains To Model End-Absorbing, Triblock Copolymers: 2. Numerical Approach†

Mikael Björling* and Peter Stilbs

Physical Chemistry, Royal Institute of Technology, SE-100 44 Stockholm, Sweden

Received November 25, 1997; Revised Manuscript Received September 21, 1998

ABSTRACT: The bridging attraction mediated by end-absorbing, triblock copolymers in a good solvent is analyzed using numerical methods and compared to analytical results. Good agreement is found. The main deviations may be attributed to the neglect of thermal fluctuations in the extension of the loops at the brush edge in the analytical treatment. With a suitable choice of "natural" units, the numerical results for the bridging probability and the free energy of interaction per chain collapse onto universal master curves in the two arrangements considered: symmetric and asymmetric adsorption of associative polymers (APs) on the surfaces of a planar slit.

I. Introduction

The previous paper of this series (hereafter referred to as paper 1 (the preceding paper in this issue)) studied the properties of end-adsorbing ABA block copolymers. In particular, a simplified model system consisting of end-confined B spacer blocks immersed in a B-type solvent in a slit was developed. Confining both spacer ends to the slit surfaces forces the spacer to adopt loop or bridge conformations, thus mimicking the behavior of a real ABA block copolymer. Since the solvent is athermal in the model, free energy changes occurring upon varying the slit width are therefore entirely of entropic origin. As in paper 1, we consider the two arrangements shown in Figure 1: asymmetric and symmetric surface coverage.

Whereas the investigation in paper 1 is based solely on analytical methods, the aim of this paper is to compare the results obtained by the numerical and analytical approaches as a function of the model parameters, i.e., slit width, spacer length and surface coverage. The numerical approach provides an independent test of scaling relationships and qualitative results predicted in paper 1, for example:

(i) The bridging attraction in the asymmetric case is orders of magnitudes stronger than the bridging attraction in the symmetric case.

(ii) When bridging spacers exist in the asymmetric case, the extension of the coexisting loop brush is proportional to the slit separation.

(iii) If the "natural" units of length and free energy are chosen in the asymmetric case, the free energy of interaction per spacer chain and the bridging probability follow universal functions that are independent of spacer length and surface coverage.

The numerical approach can also be used to resolve whether there is a set of natural units giving a universal function for the free energy of interaction also in the symmetric case. Furthermore, the validity of the additional approximations made in the analytical approach may be tested. In most cases, the numerical results presented here corroborate the analytical predictions. Since the two approaches involve different approximations, the credibility of the predictions in paper 1 is thus strengthened.

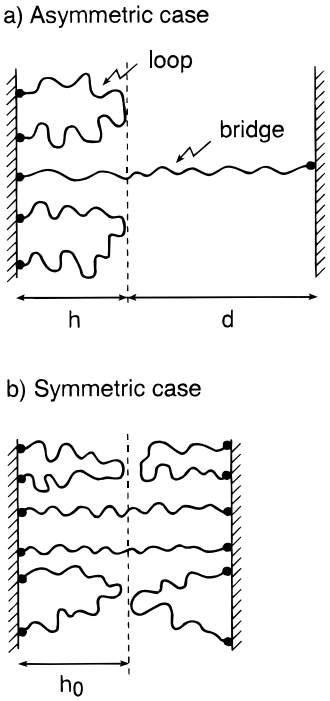

Figure 1. Schematic illustration of the asymmetric and symmetric slit.

The outline of the paper is as follows: section II describes the numerical approach (an extension of the Scheutjens−Fleer theory[1,2] with explicit constraints confining the spacer ends to the surfaces). The underlying assumptions in the two approaches are then compared, followed by a brief presentation of selected results from paper 1. Section III qualitatively discusses and compares the analytical and numerical results for a variety of system parameters: first for a single loop-covered surface and then for the asymmetric and symmetric slit, respectively. Two experimental conjectures are then discussed in section IV. The paper ends with some concluding remarks.

* To whom correspondence should be addressed.

† This paper is dedicated to the memory of Jan Scheutjens.

10.1021/ma971732n CCC: $15.00
Published on Web 11/26/1998

II. Theory

II.A. Numerical Method. The numerical method originates in the lattice-based self-consistent-field theory proposed by Scheutjens and Fleer[1,2] and has been presented in detail elsewhere.[3−5] The slit space is divided into M layers (indexed by the discrete variable i) with a thickness on the order of a unit bond length. (Note that the discrete variable i corresponds to the continuous variable z in paper 1, i.e., the distance from surface 1.) Connected spacer monomers are therefore located either in the same or adjacent layers. Due to the random-mixing approximation, a spacer conformation is represented by the ordered sequence of layers where each monomer is located. Each mean-field conformation is therefore a degenerate collection of several 3D conformations. In our simplified model, the total number of ways to place the first monomer of a specified conformation is given by the layer volume L (transverse translation). (Note that L also is the surface area since the layer thickness is unity.) Once the location of the first segment of a spacer is fixed, the remaining degeneracy can be calculated from the "connectivity" matrix λ, where each entry λ_{ij} denotes the probability to choose a connection to layer j out of all possible connections from layer i. Identifying the planar layers with layers of hexagonally close-packed spheres, the connectivity matrix is tri-diagonal with the entry's $\lambda_{i,i} = 0.5$, and $\lambda_{i,i\pm1} = 0.25$. A more elaborate, nonlattice, calculation yields the same result simply by assuming complete flexibility and random mixing.[6] However, that calculation is only strictly valid for a dimer.

When the chain ends are strongly adsorbed to the surfaces, as in this case, Wijmans et al.[7] have shown that the results for full and restricted equilibrium are virtually the same. Therefore, we only consider restricted equilibrium, that is, when the adsorbed amount is constant irrespective of the surface separation. Thus, the model system is conveniently regarded as a two or three component system consisting of solvent and one or two spacer components each associated with a slit surface (denoted 0 (solvent) and 1 or M (spacers), respectively). The asymmetric slit thus only contains spacer component 1, whereas the symmetric slit contains equal amounts of spacer component 1 and M. Introducing the surface coverage or grafting density (σ), the number of spacers per unit area, the number of each spacer component is $n_1 = \sigma_1 L$ and $n_M = \sigma_M L$. The solvent fills the rest of the volume so that $n_0 = L(M - \sigma_1 - \sigma_M)$. Indexing the consecutive spacer segments with the discrete variable s, a measure of the statistical weight (ω_{yd}) of a specific conformation d for a chain component y in the absence of interactions would be

$$\omega_{yd} = L\prod_{s=2}^{N_y}\lambda_{k(y,d,s-1),k(y,d,s)} \tag{1}$$

where $k(y,d,s)$ is the layer where segment s is located and N_y is the number of segments in component y. The direction of the sequential numbering of the segments in the spacer chain should not affect the statistical weight of a conformation. This is trivially satisfied in planar geometry by choosing $\lambda_{i,i-1} = \lambda_{i,i+1}$, as above.

When the spacers interact, each conformation d must also be properly Boltzmann weighted with a mean-field potential that replaces the strict mutual exclusion of the monomers. No *a priori* assumptions concerning the shape of the mean-field profile are made. The excluded volume interaction is instead replaced by a set of constraints that each layer is completely filled. A set of Lagrange multipliers $\{\alpha_i\}$, one for each layer, is selected so that these constraints are satisfied. Observing that the slit walls pose external exclusion constraints on the monomers, the Boltzmann weight for placing a monomer in layer i is then given by[4]

$$G_i = \exp(\alpha_i - V_i^{\text{wall}}) \tag{2}$$

where the external potential due to the slit walls $V_i^{\text{wall}} = 0$, for $i \in [1, M]$, and otherwise is infinite, so that the Boltzmann weight for placing a monomer outside the slit is zero. The component-dependent conformational constraints, i.e., loops or bridges, may also be expressed in terms of an external potential V_{ysi} confining the spacer chain ends to a surface layer. In order to control the surface coverage on each of the surfaces separately, the first segment is specified to start in one of the surface layers (cf. σ_1 and σ_M), whereas the last segment is allowed to end in either of the two. When these conformational constraints are not satisfied, the external potential is infinite.

Using eqs 1 and 2, the probability of a conformation d then becomes

$$P_{yd} = \frac{C_y}{n_y}\omega_{yd}\prod_{s=1}^{N_y}G_{k(y,d,s)}\exp(-V_{y,s,k(y,d,s)}) \tag{3}$$

where C_y/n_y is a normalizing factor. The unspecified constraint pressure profile $\{\alpha_i\}$ may, in principle, be obtained from self-consistency of eqs 3 and the volume filling constraints. However, this is impractical in the case of the spacers because the number of such equations increases very rapidly with chain length. A natural way to reduce the information content in eq 3, without losing all of the conformational details, is to calculate the contribution to the monomer density due to each segment rank (i.e. monomer index s).

The solvent component only consists of a single, unconstrained, monomer and the probability of a "conformation" reduces to the probability of placing a solvent monomer in a specific layer. The monomer density in layer i may be obtained directly from eqs 2 and 3, giving

$$\Phi_0(i) = G_i[(M - \sigma_1 - \sigma_M)/(\sum_{i=1}^{M}G_i)] \tag{4}$$

where the square bracket is C_0. Using eqs 1 and 4, we note that the Lagrange multipliers are related to the solvent monomer densities by

$$\alpha_i = \ln(\Phi_0(i)) - \ln(C_0) \tag{5}$$

at self-consistency.

For the spacers, the evaluation is less straightforward. Regrouping eq 3, it becomes apparent that the probability of a certain spacer conformation is composed of a term pertaining to the placement of the first segment ($s = 1$) and a product of weighted "step" probabilities following the "path" of that conformation.[8] This suggests the use of the transfer matrix methods commonly used for Markov chains in probability theory. Since end confinement only affects the first and last step of the random walk, the same transfer matrix $\mathbf{W}$ ($W_{ij} =$

$G_i\lambda_{ji}$) may be chosen for both spacer components. According to eq 2, the entries of **W** outside the slit are zero. Random walkers jumping through the slit walls therefore vanish. More than 30 years ago, Silberberg[9] pointed out that hard surfaces *must* be treated like absorbing boundaries (in the above manner) in order to generate the correct conformation statistics. Random walkers attempting to walk through a slit wall are not generating physical representations of chain conformations, and they, *and* their previous paths, should be given zero statistical weight. (This still deserves emphasis! Since it is intuitively appealing to choose hard walls to be reflecting, oversights of this fundamental principle are not rare.[10,11]) Only the survivors after $N - 1$ steps have followed paths that represent all admissible conformations for a chain of length N in the slit. Furthermore, the distribution of survivors after $s - 1$ steps is not the normalized distribution of segment s.

This problem is overcome by generating the chain conformations from both ends in a forward and backward walk, respectively. The true distribution of segment s is proportional to the probability that survivors after a forward walk in $s - 1$ steps meet survivors from the backward walk in $N - s$ steps.[4,12] Introducing the column vector $\mathbf{D}_i$, with entry i equal to 1 and zero otherwise, the starting vectors $\mathbf{g}_y$ for segment 1 are $LG_1\mathbf{D}_1$ and $LG_M\mathbf{D}_M$ for spacer components 1 and M, respectively. The starting vector for the last segment in the backward walk is the same for both spacer components, namely, $\mathbf{D}_1 + \mathbf{D}_M$. The contribution to the monomer density in layer i from all segments of rank s in the spacer component y is then given by[4,12]

$$\Phi_{ys}(i) = \frac{C_y}{L}[\mathbf{D}_i{}^T\mathbf{W}^{s-1}\mathbf{g}_y][\mathbf{D}_i{}^T(\mathbf{W}^T)^{N_y-s}(\mathbf{D}_1 + \mathbf{D}_M)] \quad (6)$$

where the first and second square brackets are the forward and backward walks, respectively. (Note the use of the transpose of the transfer matrix, in the backward walk.) The normalization constant in eq 6 is given by

$$C_y = n_y[(\mathbf{D}_1 + \mathbf{D}_M)^T\mathbf{W}^{N_y-1}\mathbf{g}_y]^{-1} \quad (7)$$

The total contribution of component y to the monomer density in layer i is obtained by summing eq 6 over the monomer index, i.e., $\Phi_y(i) = \sum_{s=1}^{N_y}\Phi_{ys}(i)$. Using eqs 2, 4, 6, and 7, a self-consistent set of constraint pressures $\{\alpha_i\}$ may now be determined iteratively by a Newton−Raphson procedure, so that the M volume-filling constraints $(1 - \Phi_0(i) - \Phi_1(i) - \Phi_M(i) = 0, \forall i)$ are satisfied.[3,4]

In the present paper, we are primarily interested in the bridging probability and the free energy. Equation 6 for $\Phi_{ys}(i)$ is sufficient for the simple conformational analysis required; for example, the probability of a spacer bridge from layer 1 to M is

$$\eta_1 = \Phi_{1,N_1}(M)/\sigma_1 \quad (8)$$

Note that, in this paper, "bridges" are those formed by the ends only, rather than those formed by any segments of a chain as in previous theories.[3,4] Other methods of reducing eq 3 permit a more detailed conformational analysis.[3,4] The entropic contribution to the Helmholtz free energy (the only contribution in our model) may be calculated using[4]

$$\beta F = -\beta TS = \sum_y n_y(\ln(C_y) - 1) + L\sum_i \alpha_i \quad (9)$$

where $\beta = [k_BT]^{-1}$. Since the model system is in equilibrium with bulk solvent, eq 9 is also the entropic contribution to the grand potential.[4] The free energy of interaction between two surfaces is simply the difference in free energy when two surfaces are brought from infinite separation to a separation of D layers

$$\Delta F = F(D) - F(\infty) \quad (10)$$

where infinity is any separation where the surfaces do not interact. Another property of interest is the extension of the loops on a single surface as a function of graft density and spacer length. The comparison is not entirely straightforward, but the hydrodynamic thickness may serve as a convenient measure of the "brush height". According to Scheutjens et al.[13] (see refs 13 and 14 for details), the hydrodynamic thickness is given by

$$h_H = M - \epsilon(M) \quad (11)$$

where $\epsilon(i) = (q_i \tanh(q_i{}^{-1}) + \epsilon(i - 1))/(1 + \epsilon(i - 1)(q_i{}^{-1}) \tanh(q_i{}^{-1}))$. Since $\epsilon(0) = 0$ and $q_i = [(1 - \Phi_1(i))/\Phi_1(i)]^{1/2}$, eq 11 is readily evaluated recursively for the spacer component starting in surface layer 1.

II.B. Comparison of the Numerical and the Analytical Methods. The analogy between the path of a classical particle and the conformation of a grafted polymer chain, central to the analytical method used in paper 1, is valid for long and strongly stretched chains. In the analytical approach, the mean field may vary continuously, whereas it must vary in discrete steps (the resolution is the layer width) in the numerical approach. This apparent difference vanishes in the treatment of long, grafted chains because the steps become negligibly small compared to the total brush height. The condition of strong stretching is a more severe restriction and is the main source of discrepancies between the analytical and the numerical approach.[15,16] However, it carries the advantage that the renormalization problem described in the above section is avoided.

Another crucial ingredient in the analytical method is the existence of free chain ends. Where free ends are present, the mean field must be a parabolic function $U(z) = -(A - Bz^2)$, where A and B are constants to be determined and z is the distance from the grafting surface.[17,18] In order to use the analytical method, in our AP model where the spacer ends are confined to the surfaces, free ends must therefore be artificially introduced by "cutting" loops at the midpoint to create a pair of grafted half-chains.[19] While loop midpoints are correlated, this approximation implicitly assumes that the half-chain ends are independent. No such approximation is required in the numerical approach, and in the Appendix its consequences are examined. Even though the half-chains extend further than the loops, the distribution of half-chain ends correlates fairly well to the distribution of loop midpoints.

Prescribing a parabolic form of $U(z)$ is not sufficient for a mean-field analytical solution. The constants must also be determined. While $B = \pi^2/(2N^2)$ is readily obtained for spacers of equal length $N/2$, evaluating A requires a further approximation: a relation between $U(z)$ and the local monomer density $\Phi(z)$. This relation

is intimately coupled to the solvent quality. In a marginal solvent, where the mean field is determined by the other chains rather than self-interaction, it may be argued that the mean-field $U(z)$ is proportional to $\Phi(z)$.[17] A simple analytical solution for the brush height, etc., then follows. Furthermore, the parabolic shape also applies to the monomer density profile for a grafted brush in a marginal solvent. In an athermal solvent, the mean field is proportional to $\ln(1 - \Phi(z))$ according to eq 5 above. The linear relationship proposed for a marginal solvent thus approximates an athermal solvent by using the first term in the MacLaurin series of the natural logarithm. Unfortunately, choosing a logarithmic or an even more realistic relation leads to more complicated equations that require numerical solution.[18,20]

When self-interaction becomes important, and in good solvents, it is more appropriate to use a blob picture instead of a mean field. Since the blob picture proceeds by scaling arguments, it primarily yields scaling predictions. Even though the numerical mean-field approach uses different initial approximations, we argue that it is illuminating to compare the scaling predictions from both methods in the case of an athermal solvent.

II.C. Selected Analytical and Scaling Results. Consider the brush height and the free energy of undisturbed spacer loops on a single surface. Using the half-chain approximation, it should scale similarly to that of a grafted brush. According to Milner et al.,[17] the brush height in a good solvent scales as

$$h_{0g} = C_1 N \sigma^{(1-\nu)/((d-1)\nu)} \approx C_1 N \sigma^{0.350} \tag{12}$$

and the free energy as

$$F_{0g} = C_2 N \sigma^{1/((d-1)\nu)} \approx C_2 N \sigma^{0.850} \tag{13}$$

where the subscript g is a reminder that a good solvent is assumed, N is the spacer length, σ is the number of spacers per unit area, and C_1 and C_2 are non-universal constants.[17] The last step uses the dimension $d = 3$ and the Flory exponent $\nu = 0.588$. Note that the choice of reference state for the free energy differs in the analytical and numerical approaches. In eq 13 the reference state is a bare surface (cf. eq 9).

Now consider the asymmetric case in a marginal solvent where the spacers are grafted with one end to a single slit surface and the other slit surface is bare. When the slit width is sufficiently small so that bridges to the bare surface begin to form, the analytical approach in paper 1 predicts a parabolic monomer density profile in the loop region near the grafting surface, the "parabolic" zone. Beyond the loop brush height h, no free ends exist and this "dead" zone of width d is characterized by a constant monomer density. Curiously, when loops and bridges coexist, the ratio d/h is constant and independent of N and σ. The width of the dead zone d and loop brush-height h are therefore constant fractions of the slit width D given by $d \approx 0.64307D$ and $h \approx 0.35693D$. This prediction is strictly valid for a marginal solvent but may be used as a first approximation also for the athermal solvent case. The equilibrium fraction of spacers forming bridges and the free energy of interaction per spacer chain yield universal (independent of N and σ) functions in a marginal solvent when the natural units of length and free energy are chosen. The natural unit of length and free energy turn out to be the loop brush height and the free energy per spacer of the original loop brush at infinite slit separation. This is fortunate for a conjecture to an athermal solvent. Assuming that the solvent quality does not affect the form of the universal function, the athermal results follow from a simple substitution of the natural units. The bridging probability is then given by

$$\eta_{asym} \approx 0.89921 - 0.040890\frac{D^3}{h_{0g}{}^3} \tag{14}$$

Equation 14 presupposes that bridges exist. The bridging probability is zero at $D \geq 2.8h_{0g}$ and thus gives an upper limit for the validity of eq 14. The lower limit of D is attained when the assumption of strong stretching of the loops fails. The universal free energy of interaction between the two slit surfaces *per spacer chain* is valid in the same range and is given by

$$W_{asym} = F_{asym} - F_{0g} \approx F_{0g}\left[\frac{5h_{0g}}{9D} + 0.16181\left(\frac{D}{h_{0g}}\right)^2 - 0.0027134\left(\frac{D}{h_{0g}}\right)^5 - 1\right] \tag{15}$$

The universal minimum in eq 15 is at (1.23, −0.311) in natural units.

In the symmetric case, where equal amounts of spacers are grafted on each of the slit surfaces, the free energy of interaction leads to repulsion in the classical limit (see paper 1). However, if thermal fluctuations are taken into account, a weak attraction arises when the two loop brushes nearly overlap, i.e, in the range $2h_0 - 2\xi_0 \leq D \leq 2h_0 + 2\xi_0$, where ξ_0 is the length scale of the fluctuation correction to the brush height.[19,21] In a good solvent,[21] the width of the interpenetration layer ξ_{0g} scales as

$$\xi_{0g} \sim N^{2\nu/3}\sigma^{-1/6} \approx N^{0.392}\sigma^{-1/6} \tag{16}$$

suggesting a natural, reduced separation distance, independent of N and σ, to be

$$\tilde{D} = \xi_{0g}{}^{-1}(D - 2h_{0g}) \tag{17}$$

Only the formation of bridges can lead to bridging attraction. The free energy of interaction is therefore expected to scale as the number of bridges that, in turn, scales as the number of half-chain ends located in the (relatively thin) interpenetration layer. By symmetry, ends in this region form bridges or loops with equal probability. (The fraction of bridges in the planar, symmetric case may never exceed one half.) In a good solvent, the following approximate scaling relationships are relevant for the bridging probability and the free energy of interaction per spacer chain[21]

$$\eta_{sym}(\tilde{D}) \sim (\sigma\xi_{0g}{}^2)^{-1}\tilde{\eta}_{sym}(\tilde{D}) = N^{-4\nu/3}\sigma^{-2/3}\tilde{\eta}_{sym}(\tilde{D}) \approx N^{-0.784}\sigma^{-2/3}\tilde{\eta}_{sym}(\tilde{D})$$

$$W_{sym}(\tilde{D}) \sim (\sigma\xi_{0g}{}^2)^{-1}\tilde{W}_{sym}(\tilde{D}) = N^{-4\nu/3}\sigma^{-2/3}\tilde{W}_{sym}(\tilde{D}) \approx N^{-0.784}\sigma^{-2/3}\tilde{W}_{sym}(\tilde{D}) \tag{18}$$

where $\tilde{\eta}_{sym}(\tilde{D})$ and $\tilde{W}_{sym}(\tilde{D})$ are hypothetical universal functions valid only in the interpenetration layer. The

existence of a universal function has been demonstrated for the case of a marginal solvent by Milner and Witten,[19] and in this paper we suggest that such a universal function also exists in the good solvent case. The universal interaction potential $\tilde{W}_{sym}(\tilde{D})$ obviously must start at zero for $\tilde{D} \approx 2$. At the onset of the bridging attraction, it decreases exponentially according to Milner and Witten.[19] Note that the scaling of $W_{sym}(\tilde{D})$ in eq 19 is the reverse from the asymmetric case in eq 15, where $W_{asym}(D/h_{0g}) \sim F_{0g} \sim N\sigma^{0.850}$ in a good solvent.

III. Model Results

III.A. Scaling for Loops on a Single Surface. Consider first the extension of the spacer loops on a single surface. The half-chain approximation predicts that the loop brush height scales as $N\sigma^{0.350}$ in a good solvent (eq 12). Compared to the scaling of $N^{0.588}$ for the radius of gyration of a free chain in a good solvent, the linear scaling with N implies that the end-adsorbed chains stretch significantly more. The extension of the loops is also expected to increase as the loops are increasingly crowded with increasing surface coverage, in line with the proposed scaling.

Two shortcomings of the analytically predicted parabolic monomer density profile, as compared to the numerical and the experimental profiles, is the absence of a depletion layer near the surface and an exponentially decreasing "tail" of monomer density extending beyond the classical brush height, respectively.[15] Due to smooth vanishing of the tail, the "brush thickness" becomes difficult to define, and typically it depends on the nature of the experiment. We propose to use the theoretical hydrodynamic thickness, h_H, given by eq 11 as a comparison. (In practice, the hydrodynamic thickness is supposed to be the location of the plane of zero flow velocity for a liquid flowing along a plate with attached loops.) The calculated h_H's increase perfectly linearly with chain length ($N = 20$, 50, 75, and 100) for all surface coverages tested ($\sigma = 0.05$, 0.1, 0.2, and 0.3). The empirical slopes extracted from the linear dependencies on N for each σ fit nicely to a scaling law in σ, and the extracted intercepts are fairly linear in σ ($\sigma \geq 0.1$), giving an approximate fitting equation of the form

$$h_H = 0.619\sigma^{0.39}N + 2.04\sigma - 1.46 \qquad (19)$$

For large N the first term dominates and the empirical eq 19 suggests a scaling

$$h_{0g}^{calc} = 0.619\sigma^{0.39}N \qquad (20)$$

in place of eq 12. Comparing the empirical eq 20 and eq 12, the empirical scaling exponent for σ is 0.39 as compared to the theoretical 0.35 and the constant prefactor is estimated to be $C_1 \approx 0.619$. In recent papers, Kent et al.[22] and Baranowski and Whitmore[23] question the validity of the above scaling predictions in eqs 12 and 20. They simultaneously fitted both scaling exponents to neutron reflectivity data on diblock copolymers over a wide range of N and σ and found $h_{0g} \sim N^{0.86}\sigma^{0.22}$ to be a more appropriate scaling relationship for the brush height. In view of our analysis, it is the too simple scaling relation proposed in σ that seems to be the trouble. It therefore seems unwarranted to give up the linear scaling in N that is verified both theoretically and experimentally.[22,23]

The stretching of the grafted chains is due to the crowding effect, but also to the surface itself. Even in the absence of excluded volume interaction, the end-adsorbed chains stretch significantly simply by the confinement to the positive half-space imposed by the surface (see discussion in section II.A). Numerical calculations, using eq 6 for a grafted, ideal chain, yield an average end-to-end distance scaling as $N^{0.77}$. Since a random coil end-to-end distance scale as $N^{0.5}$, the confinement imposed by the surface and the excluded volume interactions between chains contribute equally to the linear scaling of the brush height in eq 20.

The numerical free energy (eq 9) increases perfectly linearly with N as predicted by the analytical eq 13, and the extracted intercepts are linear in σ. However, the extracted slopes do not fit a scaling law in σ. The numerical free energy goes through a minimum as a function of σ due to the choice of reference state in eq 9. Fortunately, the free energy of interaction is independent of the reference state. In particular, the minima in the free energy of interaction per spacer for the asymmetric case should scale as $-0.311F_{0g}$. The numerical scaling law in σ may thus be determined by analyzing the depths of these minima. For large N, i.e., neglecting the linear dependence in σ, the numerical scaling relation is

$$F_{0g}^{calc} = 3.035N\sigma^{0.852} \qquad (21)$$

for $N = 100$ and $\sigma = 0.025$, 0.05, 0.075, and 0.1. Equation 21 is in good agreement with the asymptotic eq 13 for large N, and identification of terms gives $C_2 \approx 3.035$. For smaller N, a larger scaling exponent in σ gives a better fit, e.g., approximately $\sigma^{1.1}$, instead of $\sigma^{0.852}$ for $N = 20$.

III.B. Asymmetric Case. Some of the entropy lost due to the conformational constraints in the "stretched" loops *may* be recovered when bridges are formed to another approaching surface. The added degree of freedom leads to a bridging attraction between the surfaces.[8,24] The attraction between the surfaces is particularly strong when the approaching surface is bare. In this asymmetric case, spacers start bridging to the bare surface even though the spacers in the bridges become even more stretched than in the loop conformation. The first bridges form already at a surface separation 2.8 times the loop brush height (see paper 1). On the other hand, stretching the bridges effectively removes bridge monomers from the crowded loop region. The loop stretching is relaxed, and the overall free energy is lowered. According to the analytical treatment, in paper 1, only 28.5% of the bridge monomers reside in the loop (parabolic) region and all the rest (71.5%) reside in the dead zone. Remarkably, these fractions are completely independent of the degree of crowding (N and σ) and of the surface separation D (when loops and bridges coexist).

Another remarkable prediction, in the analytical approach, is that the loop brush height (in the presence of bridging spacers) is independent of N and σ and only depends linearly on the surface separation. In a marginal solvent, the loop brush height and the width of the dead zone are $h = 0.36D$ and $d = 0.64D$, respectively. The fact that the dead zone is wider than the parabolic zone is a consequence of the excessive stretching of the bridges, as described above. Figure 2 nicely demonstrates that these analytically predicted features

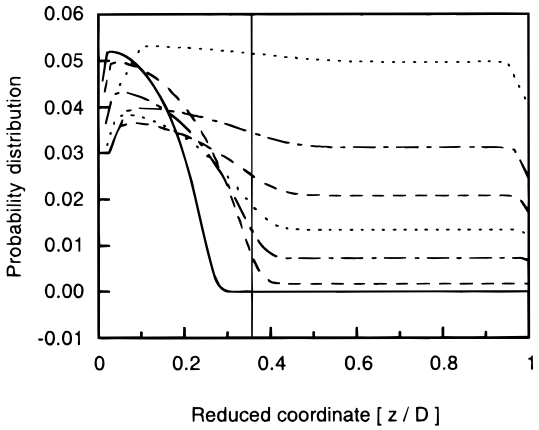

Figure 2. Probability distributions of spacer segments in an asymmetric slit versus the reduced coordinate z/D at different surface separations D, clearly showing the existence of a roughly parabolic and a dead zone ($N = 100$ and $\sigma = 0.1$). From the bottom, D is equal to 101 (full), 70 (dashed), 60 (dashed−dotted), 50 (dotted), 40 (dashed), 30 (dashed−dotted), and 20 (dotted). Note that no bridges can form at $D = 101$. The theoretical boundary (vertical line) between the parabolic and the dead zone agree rather well with the numerical density profiles except at relatively small separations.

for a marginal solvent also occur in the numerical results for an athermal solvent. A roughly parabolic zone and a dead zone are observed. The extension of the loop brush in a good solvent appears to be linear in D, even though there is evidence of a breakdown at small separations. The numerical loop brush also extends slightly past the analytical prediction of $0.36D$ (vertical line in Figure 2). The main reason for this is the neglect of thermal fluctuations in the analytical approach.[15,16] The athermal solvent may accentuate this effect, but we believe that it is of minor importance in this case.

The influence of the spacer graft density σ ($\sigma = \sigma_1$), at fixed spacer length N, on the numerically obtained bridging probability (eq 8) and free energy of interaction per spacer W ($W = \Delta F/[L(\sigma_1 + \sigma_M)]$ (where ΔF is given by eq 10) is presented in Figure 3. With increasing graft density σ, the range of the interaction increases; i.e., bridges begin to form at larger surface separations and the probability to form bridges is larger at any given separation. The decrease of the bridging probability at small separations, toward the symmetric limit of equal proportions of loops and bridges, is a consequence of a nearly isotropic constraint pressure. The deeper minima in the free energy of interaction per spacer show that the strength of the interaction increases with the surface coverage. When the loop region is crowded, it is more favorable to remove monomers from it and the probability of bridging increases.

Spacers will also experience more crowding if the spacer length N is increased at constant graft density. This is shown in Figure 4, where the bridging probability and the corresponding free energy of interaction per spacer are plotted versus D/N. As expected, the interaction is stronger and the free energy minimum becomes deeper with increasing crowding. The coinciding locations of the free energy minima and the roughly coinciding onsets of bridging confirm that the natural unit of separation scales with N. Dividing the separation by the calculated hydrodynamic radius (eq 19) does not show the same high degree of universality.

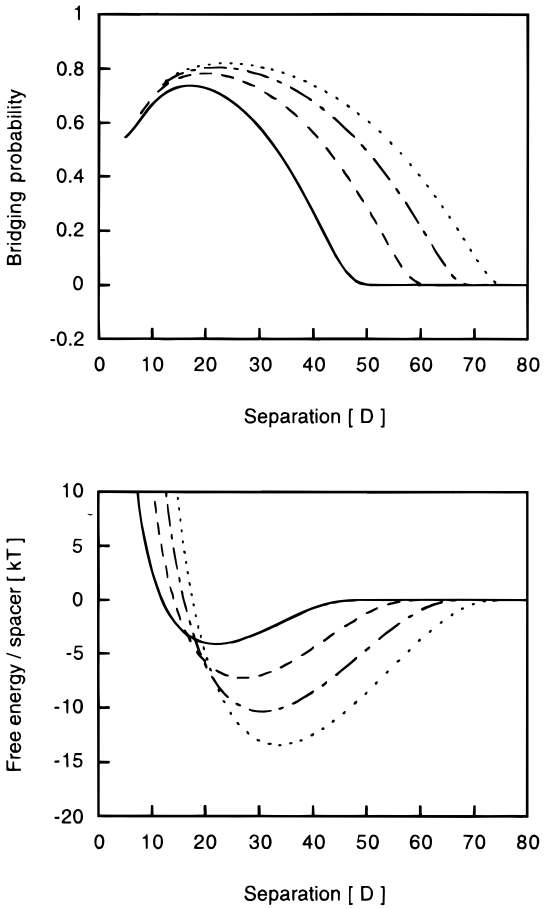

Figure 3. Bridging probability and the free energy of interaction per spacer as a function of the separation for selected graft densities (σ) in an asymmetric slit ($N = 100$). The graft densities are 0.025 (full), 0.05 (dashed), 0.075 (dashed−dotted), and 0.1 (dotted).

A more critical examination of universality in the asymmetric slit (predicted by eq 15) is to test whether the numerical curves fall onto a master curve when the appropriate natural units are used. As expected, the numerical fits of the natural units give better results than the scaling predictions. Thus, if each separation is divided by h_{0g}^{calc} and each free energy of interaction is divided by F_{0g}^{calc}, as in Figure 5, the numerical curves reduce fairly well to a master curve. Compared to the analytical master curve, the reduced numerical curves in Figure 5 are slightly shifted toward larger separations. Most of this shift is due to the classical approximation in the analytical treatment. Since the numerical brush is more extended than the analytical brush, bridges start to form at greater separations in the numerical calculations as shown in Figure 5. For the same reason, repulsion starts at greater separations. Notable deviations are also found in the bridging probability at small separations. The analytical bridging probability fails to predict the numerically observed decrease at separations approaching h_{0g}^{calc}.

When the approaching surface also bears adsorbed spacers, the tendency to form bridges and the strength of the bridging attraction decreases. This is illustrated, using the numerical approach, in Figure 6. For a slit, with a fixed amount of end-absorbing spacers, the free energy of interaction per spacer and the bridging probabilities are calculated for the asymmetric, sym-

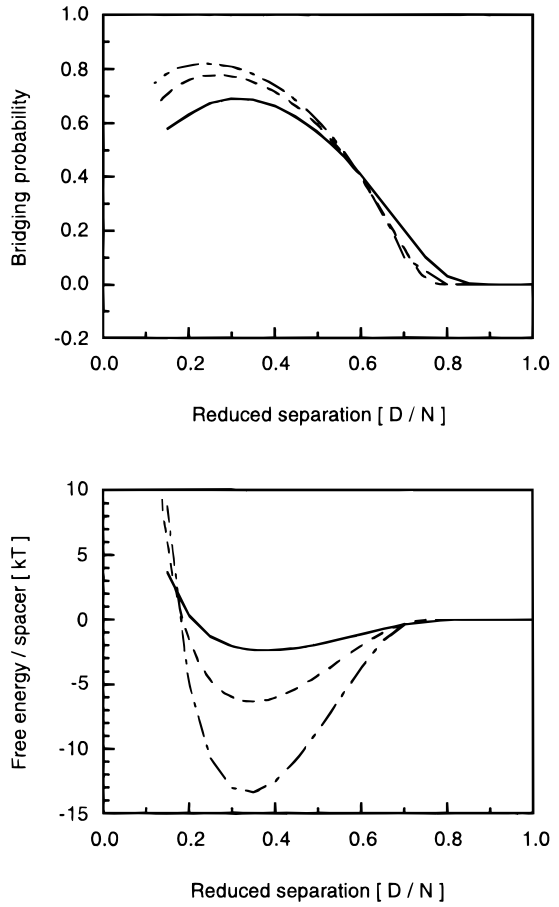

Figure 4. Bridging probability and the free energy of interaction per spacer as a function of the reduced separation for selected chain lengths (N) in an asymmetric slit ($\sigma = 0.1$). The reduced separation is D/N. The chain lengths are 20 (full), 50 (dashed), and 100 (dashed−dotted).

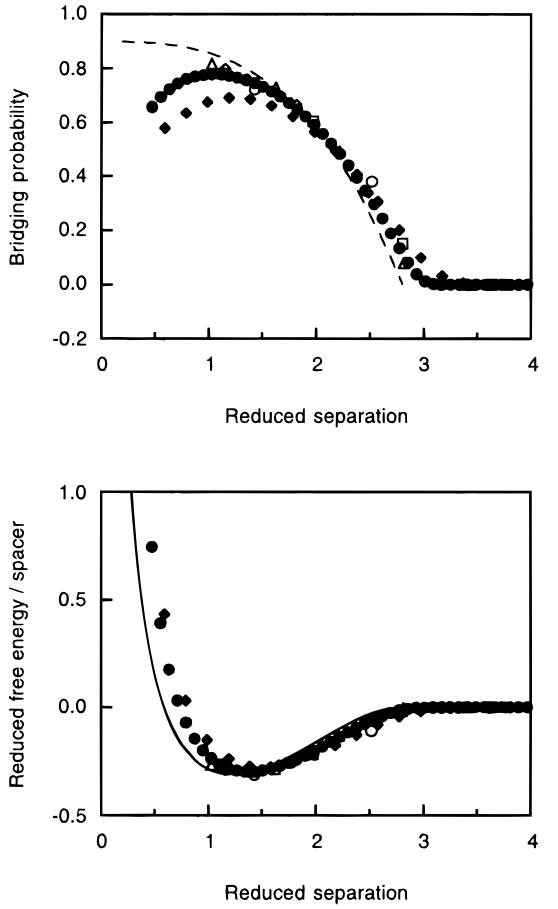

Figure 5. Numerical results for the bridging probability and the free energy of interaction per spacer in the asymmetric slit. These roughly fall on master curves when "natural" units of length (h_{0g}^{calc}, eq 20) and free energy (F_{0g}^{calc}, eq 21) are chosen. The reduced separation and free energy of interaction per spacer is D/h_{0g}^{calc} and W/F_{0g}^{calc}, respectively: for $N = 100$ and $\sigma = 0.025$ (open circles), $\sigma = 0.05$ (open squares), $\sigma = 0.075$ (open diamonds), or $\sigma = 0.1$ (open triangles); for $\sigma = 0.1$ and $N = 50$ (filled circles) or $N = 20$ (filled diamonds). The theoretical master curves for the free energy of interaction per spacer (full line) and the bridging probability (dashed line) are included for comparison.

metric, and intermediate cases. (Note that the bridging probabilities in Figure 6a (top) refer only to chains on the surface with the most chains.) The probability of bridging chain ends and the bridging attraction decreases dramatically as the equilibrium symmetric case is approached. In order to use the asymmetric system in adhesive applications, the asymmetry must therefore be preserved by grafting one of the spacer ends to the surface.

III.C. Symmetric Case. Finally, we examine the properties of a fully equilibrated system where the surfaces have equal amounts of adsorbed spacers. Figure 7 shows the bridging probability and the free energy of interaction per spacer (see III.B) for different graft densities σ ($\sigma = \sigma_1 = \sigma_M$), while maintaining constant chain length. While the range of the interaction increases with increasing surface coverage, the free energy minimum per spacer becomes more shallow. (Note, however, that the minimum in the free energy of interaction per unit surface becomes deeper with increasing surface coverage (not shown). Each spacer contributes less, but is overcompensated by the increase in the number of contributing spacers.) Comparing Figures 3 and 7, it is obvious that the interaction in the symmetric case is much weaker than in the asymmetric case, as predicted in paper 1. Nevertheless, formation of bridges is favorable for the same reason in both cases, i.e., removal of monomers from the crowded loop region. However, in contrast to the asymmetric case, the number of spacer ends on each surface is equal and constant in the symmetric case. By symmetry, a spacer end removed from one surface to form a bridge to the other surface is compensated by a spacer end coming from a bridge in the reverse direction. The bridges in the symmetric case therefore only relieve crowding in the loop region by increasing the monomer density in the mid-plane region. The available mid-plane region is gauged by the width of the interpenetration layer (eq 16) in which the bridging attraction in the symmetric case may occur. Since the width of the interpenetration layer decreases with increasing graft density, each bridge is less effective in relieving the crowding and consequently gives a smaller contribution to the bridging attraction. The decreasing widths of the minima in Figure 7 also reflect the decreasing widths of the interpenetration layer with increasing graft density.

The effect of chain length at constant graft density is shown in Figure 8, where the reduced separation is D/N. As the chain length increases, fewer bridges are formed and the bridging attraction becomes weaker. The decreasing strength of the bridging attraction and the

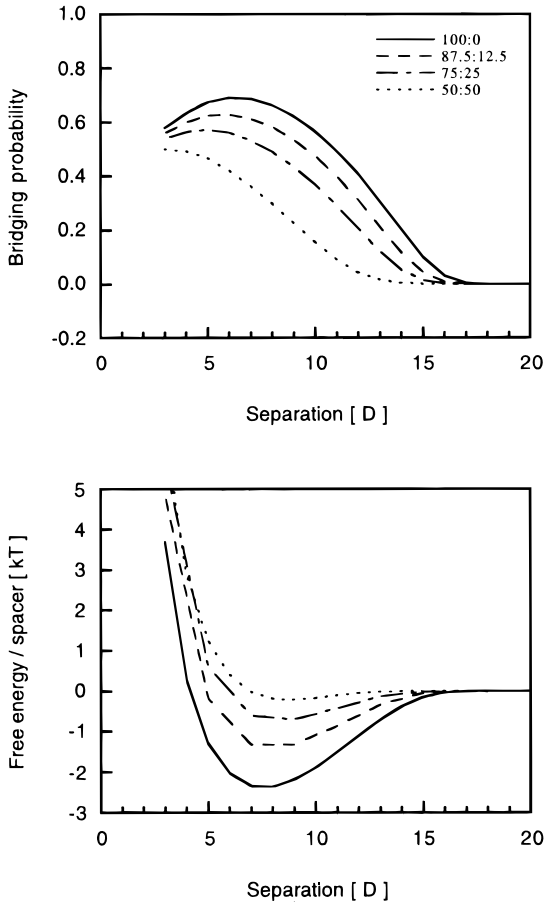

Figure 6. Bridging probability and the free energy per spacer as a function of separation as the slit progressively changes from the totally asymmetric (100:0) to the symmetric (50:50) adsorption. The total number of spacers ($N = 20$) in the slit is constant and corresponds to $\sigma = 0.1$ for the totally asymmetric (or to $\sigma = 0.05$ for the symmetric) slit. The percentages of spacers forced to reside on either surface for the intermediate cases are 87.5:12.5 and 75:25 (see legend).

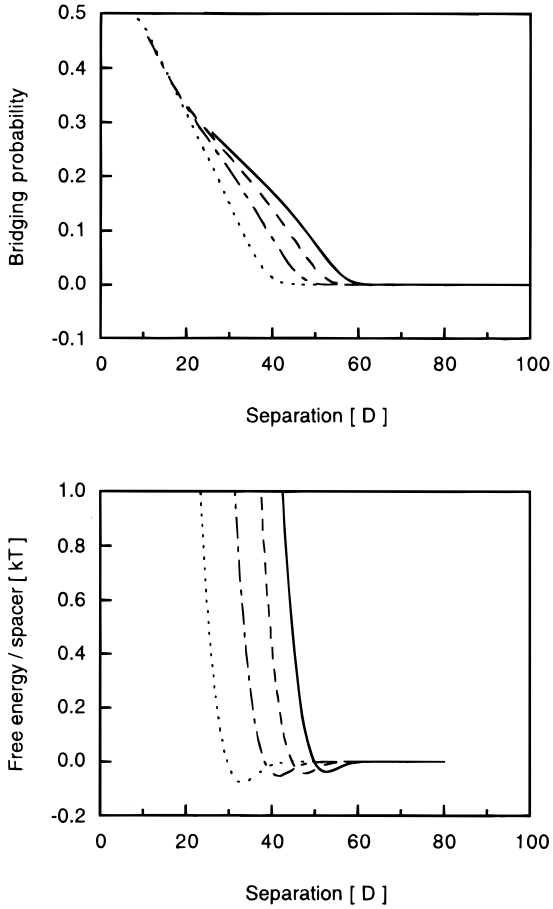

Figure 7. Bridging probability and the free energy of interaction per spacer as a function of the separation for selected graft densities (σ) in a symmetric slit ($N = 100$). The graft densities are 0.025 (dotted), 0.05 (dashed−dotted), 0.075 (dashed), and 0.1 (full).

relative width of the free minima upon increasing N reflect a corresponding decrease of the width of the interpenetration layer.

A universal function for the symmetric case is not known a priori, but Milner and Witten[19] has shown that it is likely to exist in a marginal solvent. Figure 9 demonstrates that such a function seems to exist also in an athermal solvent. The numerical natural unit of free energy per spacer appears close to the scaling prediction $(\sigma\xi_0^2)^{-1}$. However, a significantly better reduction to a master curve was obtained using h_{0g}^{calc} in eq 17, that is, with the reduced separation given by $\tilde{D} = \xi_{0g}^{-1}(D - 2h_{0g}^{calc})$.

IV. Comparison with Experiments

An obvious experimental analogy to the calculated interactions above is a surface force experiment. Figure 6 is in fact meant to illustrate the force measurements of Dai et al.[25−27] They succeeded in adsorbing triblock copolymers (PEO-PS-PEO and PVP-PS-PVP in toluene, where PEO = poly(ethylene oxide), PS = polystyrene, and PVP = polyvinylpyrrolidone) onto a single mica surface. Inserting a second, fresh mica surface enabled them to measure forces between a surface with end-adsorbed triblock copolymers and a bare surface. The measured forces are initially strongly attractive, but after each compression−decompression cycle they grow weaker and weaker.

The numerical results in Figure 6 imply a simple rationalization, also suggested by Dai et al., of the observed experimental results. At the outset, the ABA block copolymers are asymmetrically adsorbed in the slit and the bridging attraction is strong. For each compression−decompression cycle the slit approaches the equilibrium state of even adsorption by depositing more and more triblock copolymers on the "bare" mica surface. The bridging attraction thus decreases. The strongly end-absorbing PVP-PS-PVP correspond most closely to the model of end-confined chains in Figure 6 and show a weak attraction at equilibrium. The purely repulsive experimental force obtained at equilibrium for PEO-PS-PEO[25,26] is possibly due either to the existence of dangling, nonadsorbed spacer ends or to the presence of small amounts of diblocks in the triblock sample. Both lead to dangling tails of length N, and the steric repulsion mediated by these is sufficiently strong and of sufficient range to kill the small attractive contribution from the end-adsorbed triblocks. In this case,[27] nonadsorbed spacer ends seem to be the likely candidate.

A second analogy is of some practical interest and concerns the stability of particle dispersions. Figure 8 implies that particle dispersions at equilibrium (i.e., the symmetric case) are less likely to flocculate when the end-absorbed APs have long, rather than short, spacers.

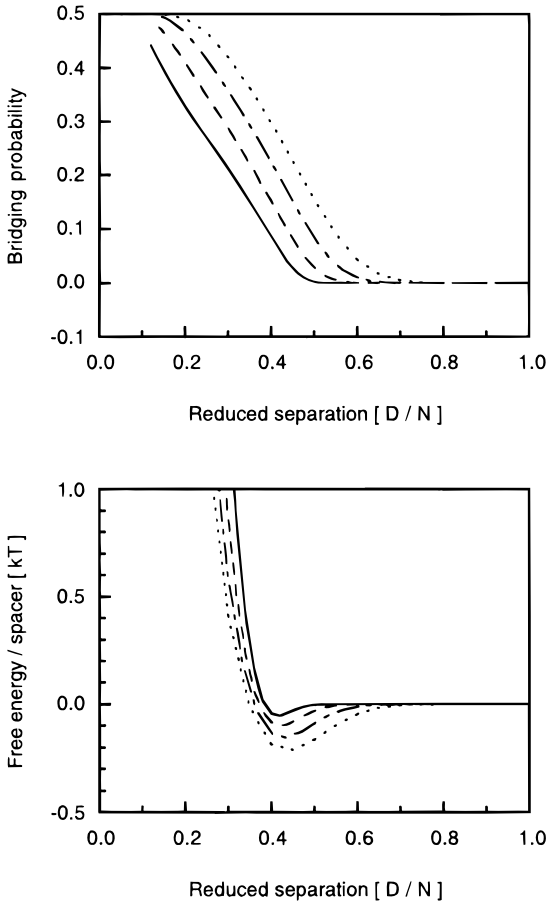

Figure 8. Bridging probability and the free energy of interaction per spacer as a function of the reduced separation for selected chain lengths (N) in a symmetric slit ($\sigma = 0.1$). The reduced separation is D/N. The chain lengths are 20 (dotted), 30 (dashed−dotted), 50 (dashed), and 100 (full).

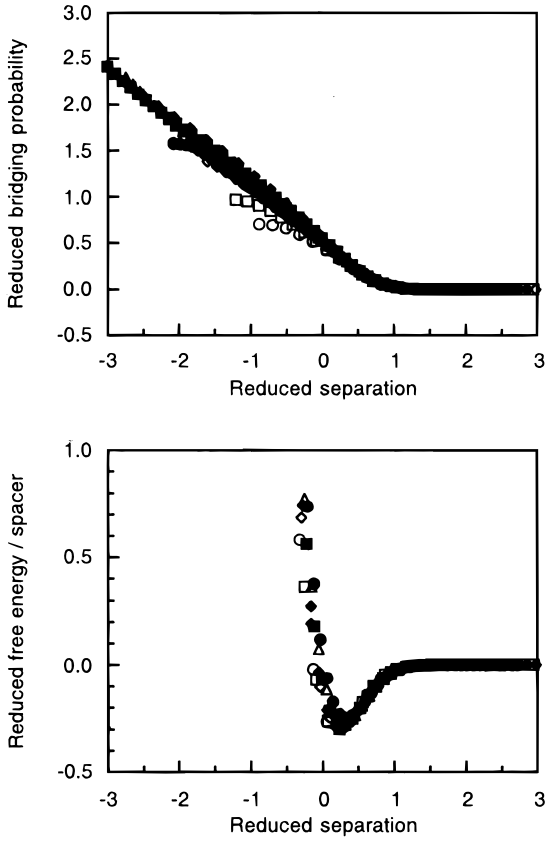

Figure 9. Numerical results for the bridging probability and the free energy of interaction per spacer in the symmetric slit. These roughly fall on master curves when "natural" units of length and free energy are chosen. The reduced separation is $(D - 2h_{0g}^{calc}/\xi_{0g}$ (cf. eq 17). The reduced bridging probability and free energy of interaction per spacer is (eq 18) $\eta\sigma\xi_{0g}^2$ and $W\sigma\xi_{0g}^2$, respectively: for $N = 100$ and $\sigma = 0.025$ (open circles), $\sigma = 0.05$ (open squares), $\sigma = 0.075$ (open diamonds), or $\sigma = 0.1$ (open triangles); for $\sigma = 0.1$ and $N = 50$ (filled circles), $N = 30$ (filled squares), or $N = 20$ (filled diamonds).

On the other hand, Figure 5 shows that this is precisely the most unstable situation in the asymmetric case, for example, in the presence of bare particles. The analytical treatment of the symmetric and the asymmetric cases correspondingly predicts reverse scaling of the free energy of interaction per unit area with respect to N, that is, $N^{-0784}\sigma^{1/3}$ and $N\sigma^{1.850}$, respectively. This reverse scaling is probably one of the reasons for the inconvenient sensitivity to changes in the formulation of water-based paints containing APs. Ideally, paints of different colours are obtained simply by adding the appropriate pigments to a common paint base consisting of a stabilized latex dispersion and small amounts of APs. However, the above considerations suggest that flocculation may be induced if the added pigment particles are bare. Pretreatment of pigments with APs, prior to the addition to the paint base, could prevent flocs that are difficult and/or slow to redisperse.

V. Conclusions

A numerical approach to model associative triblock copolymers as end-absorbing chains is presented, and its results are compared to analytical and scaling predictions. A useful symbiosis of the two methods is observed. The analytical treatment provides a framework in which the numerical results are easier to rationalize. The numerical approach, on the other hand, involves less severe and different approximations and may critically test the analytic assumptions and predictions. The numerical results for a loop system and a corresponding system of half-chains are, for example, found to be in acceptable agreement (Appendix). A crucial approximation in the analytical treatment is therefore well-founded.

The numerically calculated hydrodynamic thickness, related to the extension of the loops, is found to be perfectly linear in N (eq 19). On the other hand, a simple scaling relationship in σ for the hydrodynamic thickness is not supported unless N is very large. The numerical scaling prediction for the loop brush height, including the constant prefactor, then becomes $0.619N\sigma^{0.39}$ (eq 20). This should be compared to the scaling prediction $N\sigma^{0.35}$ (eq 12) in the half-chain approximation. The scaling prediction for the free energy per loop in a good solvent $N\sigma^{0.85}$ (eq 13), also agrees quite well with the numerical prediction $3.035N\sigma^{0.852}$ (eq 21). An advantage of the numerical approach is the rough estimates of the prefactors.

For the asymmetric slit, the numerically calculated monomer density profiles indeed support a division into a parabolic and a dead zone, as suggested by the analytical treatment in paper 1. Furthermore, using the numerical "natural" units of length and free energy, the numerical data do fall on a universal master curve. The main deviations between the analytical and the

numerical predictions are due to the classical approximation, neglecting k_BT fluctuations in the extension of the loops in the analytical treatment.

Even though the asymmetric slit is an interesting special case, the symmetrical case is the equilibrium situation for physically adsorbed associative polymers. In line with the predictions by Kosmas et al. for Gaussian chains,[11] we find that the bridging attraction in the symmetric slit is much weaker than in the asymmetric slit. This is also corroborated by the analytical predictions in paper 1. Our numerical calculations also support the same scaling relationship for the natural unit of free energy per spacer and bridge probability in a good solvent as suggested by Semenov et al.,[21] i.e., $N^{-0.784}\sigma^{-2/3}$ (eq 18). Using a reduced separation scaling such as $N^{-0.392}\sigma^{1/6}(D - 1.238N\sigma^{0.39})$, the reduction of the numerical data onto a universal master curve is quite good (Figure 9). An approximate universal function for the free energy of interaction per spacer, previously shown to exist in a marginal solvent,[19] therefore seems to exist also in a good solvent (Figure 9).

In summary, good agreement is found between the analytical and numerical results in spite of the different approximations involved.

Acknowledgment. We thank Jan-Christer Eriksson for helpful comments on the manuscript. This work was supported by the Swedish Natural Science Research Council (NFR), the Swedish Research Council for Engineering Sciences (TFR), and Magnus Bergwalls Stiftelse.

Appendix

In this appendix, the necessary approximations required for replacing the monomer density profile of a loop with that of two half-chains are critically examined. We start by rewriting eq 6 for the total monomer density for loops of length N in order to expose its underlying half-chain symmetry. Dividing the second square bracket in eq 6 and eq 7 into two parts by inserting the identity matrix in the form of $\mathbf{I} = \sum_{j=1}^{M}\mathbf{D}_j\mathbf{D}_j^{\mathrm{T}}$ after $N/2$ steps yields

$$\Phi_1(i) = 2\sigma_1\sum_{s=1}^{N/2}\frac{\{[\mathbf{D}_i^{\mathrm{T}}\mathbf{W}^{s-1}\mathbf{D}_1]\sum_{j=1}^{M}[\mathbf{D}_i^{\mathrm{T}}(\mathbf{W}^{\mathrm{T}})^{N/2-s}\mathbf{D}_j][\mathbf{D}_1^{\mathrm{T}}\mathbf{W}^{N/2}\mathbf{D}_j]\}}{\{\sum_{j=1}^{M}[\mathbf{D}_j^{\mathrm{T}}\mathbf{W}^{N/2-1}\mathbf{D}_1][\mathbf{D}_1^{\mathrm{T}}\mathbf{W}^{N/2}\mathbf{D}_j]\}} \quad \text{(A1)}$$

where the transpose of the scalars in the square brackets may be taken freely. (Note that eq A1 implies that N is even or very large.) Now imagine cutting the loops at the midpoints into two half-chains of length $N/2$. If the artificially introduced half-chain ends are considered "free", or independent of each other, the loop constraints are lifted. The sum over products in eq A1 is transformed into a product of sums and simplifies to

$$\Phi_1(i) = 2\sigma_1\sum_{s=1}^{N/2}\frac{[\mathbf{D}_i^{\mathrm{T}}\mathbf{W}^{s-1}\mathbf{D}_1][\mathbf{D}_i^{\mathrm{T}}(\mathbf{W}^{\mathrm{T}})^{N/2-s}\mathbf{s}]}{[\mathbf{s}^{\mathrm{T}}\mathbf{W}^{N/2-1}\mathbf{D}_1]} \quad \text{(A2)}$$

Equations A1 and A2 obviously differ. The severity of approximating the loops by two half-chains with free ends may be demonstrated using the numerical approach in two test cases (*a*, $N = 20$, $\sigma = 0.2$; *b*, $N = 100$, $\sigma = 0.1$).

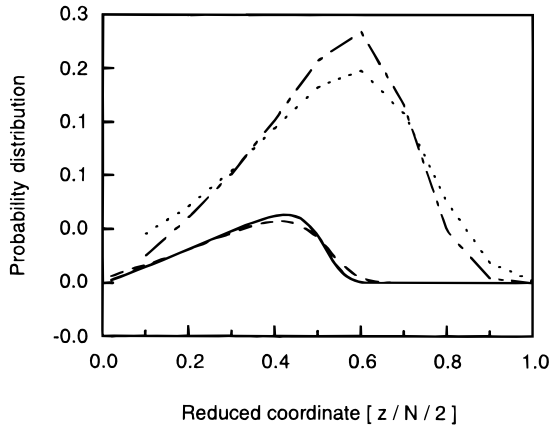

Figure 10. Middle segment distribution for loops of length N on a single surface and the end segment distribution for the corresponding system of two half-chains of length $N/2$ when $N = 100$ (loops (full) and half-chains (dashed)) and when $N = 20$ (loops (dashed−dotted) and half-chains (dotted)). The graft density for the spacers corresponds to $\sigma = 0.1$ and $\sigma = 0.2$ for $N = 100$ and $N = 20$, respectively.

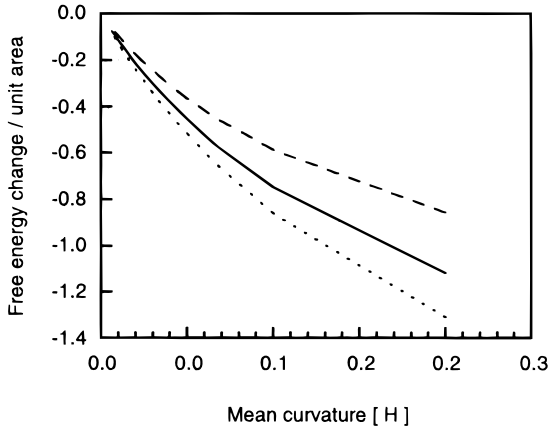

Figure 11. Effect of curvature on the half-chain approximation. The change of free energy per unit surface upon cylindrical bending of a planar surface toward the insoluble A phase for loops $N = 20$ and $\sigma = 0.2$ (full) and for the corresponding half-chain system (dotted). The mean curvature is given by $H = 0.5(1/R)$, where R is the radius of curvature of the cylinder. The comparable AB diblock system, i.e., grafted chains with $N = 20$ and $\sigma = 0.2$ (dashed), is also shown for comparison.

The free energy of the system obviously must decrease when the loop constraint is lifted. Comparing the calculated free energies shows a decrease to be 18 and 2% for cases a and b, respectively. Figure 10 shows that the distribution of half-chain ends and loop midpoints are roughly equal in both cases but confirms that the approximation is worse for case a. Nevertheless, Figure 10 demonstrates that the half-chain approximation is acceptable.

The half-chain approximation is also expected to be less good in predicting free energy changes when the surface curvature varies. (Surface curvature is easily introduced in the numerical approach by modifying the connectivity matrix.[3−5]) In Figure 11 we examine the consequences of three different types of end confinements: (i) spacers with one end confined to the surface (an AB diblock); (ii) spacer loops with both ends confined to the surface; (iii) spacers cut into half-chains with one

end confined to the surface. The adsorbed amount and the "spacer" length are kept constant. Figure 11 shows the free energy changes per unit surface as a function of curvature upon cylindrical bending of a planar surface toward the insoluble A phase. It clearly is easier to cylindrically bend a surface with grafted half-chains toward the insoluble A phase than to bend a corresponding surface with loops. A surface with loops is easier to bend than the corresponding surface with diblocks.

References and Notes

(1) Scheutjens, J. M. H. M.; Fleer, G. J. *J. Phys. Chem.* **1979**, *83*, 1619.
(2) Scheutjens, J. M. H. M.; Fleer, G. J. *J. Phys. Chem.* **1980**, *84*, 178.
(3) Evers, O. A.; Scheutjens, J. M. H. M.; Fleer, G. J. *Macromolecules* **1990**, *23*, 5221.
(4) Björling, M. *Macromolecules* **1992**, *25*, 3956.
(5) Linse, P.; Björling, M. *Macromolecules* **1991**, *24*, 6700.
(6) Björling, M.; Linse, P. *J. Chem. Phys.* **1992**, *97*, 6890.
(7) Wijmans, C. M.; Leermakers, F. A. M.; Fleer, G. J. *J. Colloid Interface Sci.* **1994**, *167*, 124.
(8) Dimarzio, E. A.; Rubin, R. *J. Chem. Phys.* **1971**, *55*, 4318.
(9) Silberberg, A. *J. Phys. Chem.* **1962**, *66*, 1872.
(10) de Gennes, P.-G. *Scaling Concepts in Polymer Physics*; Cornell University Press: Ithaca, NY, 1979; Chapter I.1.
(11) Kosmas, M.; Tenbrinke, G.; Hadziioannou, G. *J. Phys. II* **1994**, *4*, 501.
(12) Björling, M.; Linse, P.; Karlström, G. *J. Phys. Chem.* **1990**, *94*, 471.
(13) Scheutjens, J. M. H. M.; Fleer, G. J.; Cohen Stuart, M. A. *Colloids Surf.* **1986**, *21*, 285.
(14) Cohen Stuart, M. A.; Waajen, F. H. W. H.; Cosgrove, T.; Vincent, B.; Crowley, T. L. *Macromolecules* **1984**, *17*, 1825.
(15) Milner, S. T. *J. Chem. Soc.* **1990**, *86*, 1349.
(16) Wijmans, C. M.; Scheutjens, J. M. H. M.; Zhulina, E. B. *Macromolecules* **1992**, *25*, 2657.
(17) Milner, S. T.; Witten, T. A.; Cates, M. E. *Macromolecules* **1988**, *21*, 2610.
(18) Zhulina, E. B.; Borisov, O. V.; Priamitsyn, V. A. *J. Colloid Interface Sci.* **1990**, *137*, 495.
(19) Milner, S. T.; Witten, T. A. *Macromolecules* **1992**, *25*, 5495.
(20) Shim, D. F. K.; Cates, M. E. *J. Phys. (Paris)* **1989**, *50*, 3535.
(21) Semenov, A. N.; Joanny, J.-F.; Khokhlov, A. R. *Macromolecules* **1995**, *28*, 1066.
(22) Kent, M. S.; Lee, L. T.; Factor, B. J.; Rondelez, F.; Smith, G. S. *J. Chem. Phys.* **1995**, *103*, 2320.
(23) Baranowski, R.; Whitmore, M. D. *J. Chem. Phys.* **1995**, *103*, 2343.
(24) Scheutjens, J. M. H. M.; Fleer, G. J. *Macromolecules* **1985**, *18*, 1882.
(25) Dai, L.; Toprakcioglu, C. *Europhys. Lett.* **1991**, *16*, 331.
(26) Dai, L.; Toprakcioglu, C. *Macromolecules* **1992**, *25*, 6000.
(27) Dai, L. M.; Toprakcioglu, C.; Hadziioannou, G. *Macromolecules* **1995**, *28*, 5512.

MA971732N